

SK-L2V2 (4/05/85)

LS-20
AUS-26

MODIFIED ALADDIN LATTICE L2V2

S. Kramer and Y. Cho

The N30 lattice discussed in a previous note showed that a nearly matched lattice could be produced by separating four of the present quadrupole from their present power supplies and powering them separately. Although having significantly higher dynamic aperture, less closed orbit distortion and improved natural emittance compared to the present Aladdin lattice, the proximity of the $v_x = 5.24$ tune was felt to be too close to the $3v_x = 16$ (a structure resonance) and the tune should be raised.

In order to demonstrate the tuneability of this modified lattice, Yang Cho found a new tune ($v_x = 6.27$, $v_y = 6.23$), hereafter called L2V2 lattice. This lattice, although not as nicely matched as the N30 lattice, has a 10% lower natural emittance and considerably more dynamic aperture. The L2V2 lattice has not been fully optimized, but is sufficient to demonstrate the advantages of this modified Aladdin lattice.

Linear Lattice Properties

The linear lattice functions for the L2V2 lattice are shown in Fig. 1(a). A comparison of the linear and first order properties of this lattice with the present Aladdin (Synch) and N30 lattice is presented in Table 1. Figure 1(b) shows the phase advance through a single L2V2 period. A nice feature of this lattice is the 90° phase advance between the center of the straight section and the short straight after the triplets. This feature would allow easy injection into the long straight section using only a pair of bump magnets.

Figure 2 shows the tune diagram for the L2V2 lattice with a $\pm 1\%$ momentum variation included. Dashed lines indicate the second and third order resonances while fourth order are indicated with dotted lines. The proximity to the $2v_x + 2v_y = 25$ should not be a problem, however, the tune could be reduced closer to $v_x = 6.20$ if desired, with some loss of symmetry between the beam lines. Figure 3 shows the tune variation with momentum which is well

behaved and doesn't cross the $v_x = 6.25$ line for $\pm 1\%$ momentum error. Variations¹ of β_x , β_y and η with momentum in the straight section are shown in Figure 4. The ratio¹ of β_x and β_y for a 1% momentum change is shown in Figure 5 for the complete cell. This momentum error corresponds to 17 times the natural momentum error. The horizontal appears well behaved while the vertical will require special care to avoid beam loss due to the larger beam at injection.

Figure 6 shows the RMS orbit displacements as calculated by the program PATRIS² for this lattice assuming, a bending magnet mispowering of $\Delta\theta_{rms} = 0.1$ mrad and quadrupole misplacements of $\Delta y_{rms} = \Delta x_{rms} = 0.1$ mm. The sensitivity to these errors is a factor of two less for the horizontal and about a factor of three less in the vertical, compared to the present Aladdin lattice. Compared to the N30 lattice, the horizontal distortions are similar while the vertical has increased about 30% for the L2V2 lattice.

Aperture Studies

The dynamic aperture was studied for the L2V2 lattice using the PATRICIA 84.9 program³ and the program PATRIS² which agreed to better than 10%. Particles were tracked for 1000 turns and considered stable if they survived a 1 meter aperture test at each sextupole. All particles were started with $x' = y' = 0$ and an amplitude $x = N_x \sqrt{\epsilon_0 \beta_x} = N_x \sigma_x$ and $y = N_y \sqrt{\epsilon_0 \beta_y} = N_y \sigma_y$ with ϵ_0 = the natural emittance in the horizontal with zero coupling. Although this overestimates the rms physical beam size by $\sqrt{2}$ (for full coupling), this definition has been used frequently in the Aladdin Upgrade Report. Figure 7 shows the dynamic aperture, the N_x vs N_y limit of stability, for $\delta p/p = 0$, $\delta p/p = +0.3\%$ and $\delta p/p = -0.3\%$. Although the aperture has increased significantly compared to the N30 lattice, considerably more variation of the aperture with momentum is observed. The solid lines indicate the linear physical acceptance of this lattice.

Figure 8 shows the phase space trajectories for a particle which is near the dynamic aperture limit. The particle trajectory is observed in the center of the long straight section, where $x = 3.75$ mm corresponds to $N_x = 10$ and $y = 4.19$ mm corresponds to $N_y = 10$. Figure 9 shows the dynamic aperture for $\delta p/p = \pm 0.6\%$ which corresponds to 10 times the natural momentum spread

for this machine. Once again, the momentum dependence is observed and has become somewhat larger.

There is a comfortable margin between the dynamic aperture for stability and the linear physical aperture for this machine. The physical limits of the vacuum chamber have been assumed square with ± 35 mm in the quadrupoles. However, the broadening of the phase space ellipse seen in Figure 8 indicates that the real physical aperture for this lattice will be less than that shown in Figures 7 and 9. By inserting zero strength sextupoles near the physical aperture limits of the machine (Q1 in horizontal plane and Q2X in the vertical/plane) a test can be made on the particle position $|x| \leq 35$ mm and $|y| \leq 35$ mm. In fact, a test at all sextupoles was made with these same limits and any particle that survived 1000 turns was considered stable. Of course, no multiple scattering, intrabeam scattering or quantum fluctuations are included in these tracking runs, which would tend to reduce the physical aperture even further. However, the physical aperture seems quite adequate to provide excellent beam lifetime once the closed orbit distortions are reduced to 2 mm or less in the ring. From Figure 6, this requires the positional accuracy or corrections to be at least 0.1 mm. The influence of a nonzero n at the aperture limits and the distorted particle trajectory in the horizontal (e.g., Figure 8), yield slightly more horizontal aperture for $\delta p/p = 0$ and -0.6%. The decreased vertical aperture for negative $\frac{\delta p}{p}$ is due to the increased β_y ($\approx 15\%$ increase at Q2X for $\delta p/p = 0.6\%$). Figure 11 shows the physical aperture for a $\delta p/p = 0.6\%$ momentum error which includes synchrotron oscillations as calculated by the PATRICIA 84.9 program.³ The 1000 turns correspond to a 1.2 synchrotron period and this aperture agrees to within 10% of the $\delta p/p = 0$ aperture, except for the points at $N_x = 35$ and 40.

References

- 1 The variation of the Twiss parameters with momentum were calculated using the CERN program MAD (version 3.06) and agree with the PATRICIA calculations. MAD is the Methodical Accelerator Design program by F. Christoph Iselin, Reference Manual LEP Division Nov. 1, 1984.
- 2 PATRIS is the tracking program by A. Ruggiero private communication.
- 3 PATRICIA 84.9 is the latest tracking code generated by H. Weideman - SSRL ACD-Note No. 22, November 1984.

Table 1
Comparison of ALADDIN Lattices

Function	ALADDIN Synch Lattice	ALADDIN N30 Lattice	ALADDIN L2V2 Lattice
$\frac{dx}{dt}$	7.135	5.236	6.270
$\frac{dy}{dt}$	7.095	6.281	6.231
ξ_x (Chromaticity)	-10.809	-7.630	-8.847
ξ_y "	-19.245	-10.456	-12.775
K_z (SF)	-2.465	-1.982	-2.481
K_z (SD)	5.576	5.320	6.385
Horiz. Damping time	13.9	13.9	13.9 msec
ϵ (natural)	164	117	103 $\times 10^{-9} m$
$\epsilon_{P/P}$ (natural)	0.059%	0.059%	0.059%
α_x (long straight)	-0.577	0	0.035 m
α_x (" ")	-1.055	0	-0.028
α_y (" ")	-0.033	0	-0.004
B_x (max) (location)	11.68 (Q3)	7.552 (Q1)	7.467 (Q1) m
B_y (max) (location)	16.41 (Q2)	10.282 (Q2)	12.919 (Q2) m
B_x (Bend)	2.183 ± 0.628	1.469 ± 0.006	1.424 ± 0.015 m
B_y (Bend)	2.340 ± 0.354	2.205 ± 0.053	2.119 ± 0.057 m
E_x (max.) physical	101.5 (Q3)	162.2 (Q1)	$153.4 (Q1) \times 10^{-6} n$
E_y (max.) physical	69.9 (Bend)	108.5 (Bend)	$91.8 (Q2) \times 10^{-6} r$
$K(QF)$	-5.300977	-5.5916950	-5.768874
$K(QD)$	5.480832	5.1741640	5.472590
$K(Q1)$	-4.600982	-2.850929	-3.254490
$K(Q2)$	5.618463	4.1141180	5.117563
$K(Q3) = K(Q3X)$	-4.651147	-2.0465900	-3.283341
$K(Q1X)$	—	-1.4831900	-1.610238
$K(Q2X)$	—	3.8871980	4.134007
$K(QFX)$	—	-4.0516260	-3.747761
$K(QDX)$	—	4.8239590	3.651153

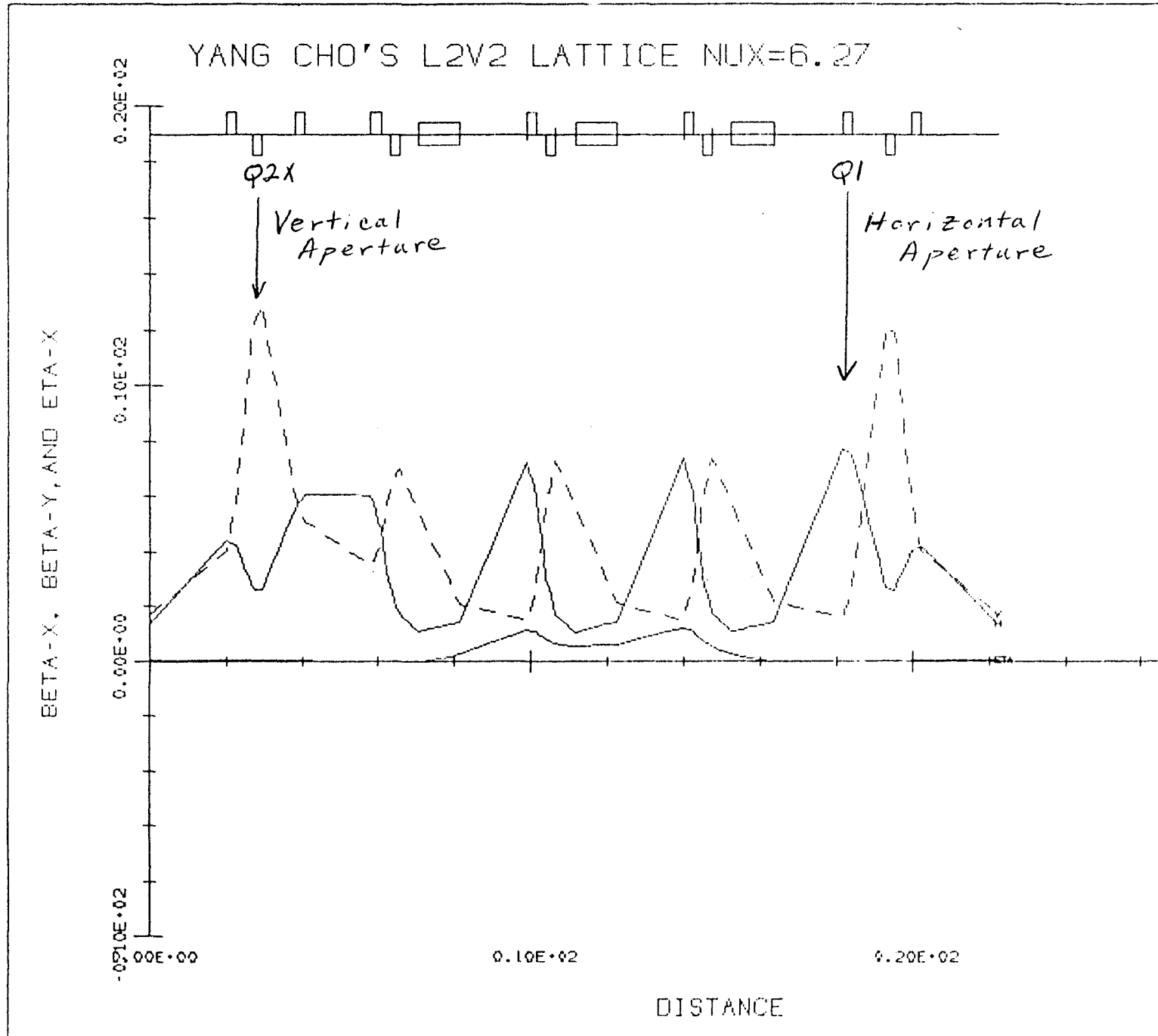


Figure 1(a). L2V2 Lattice Functions

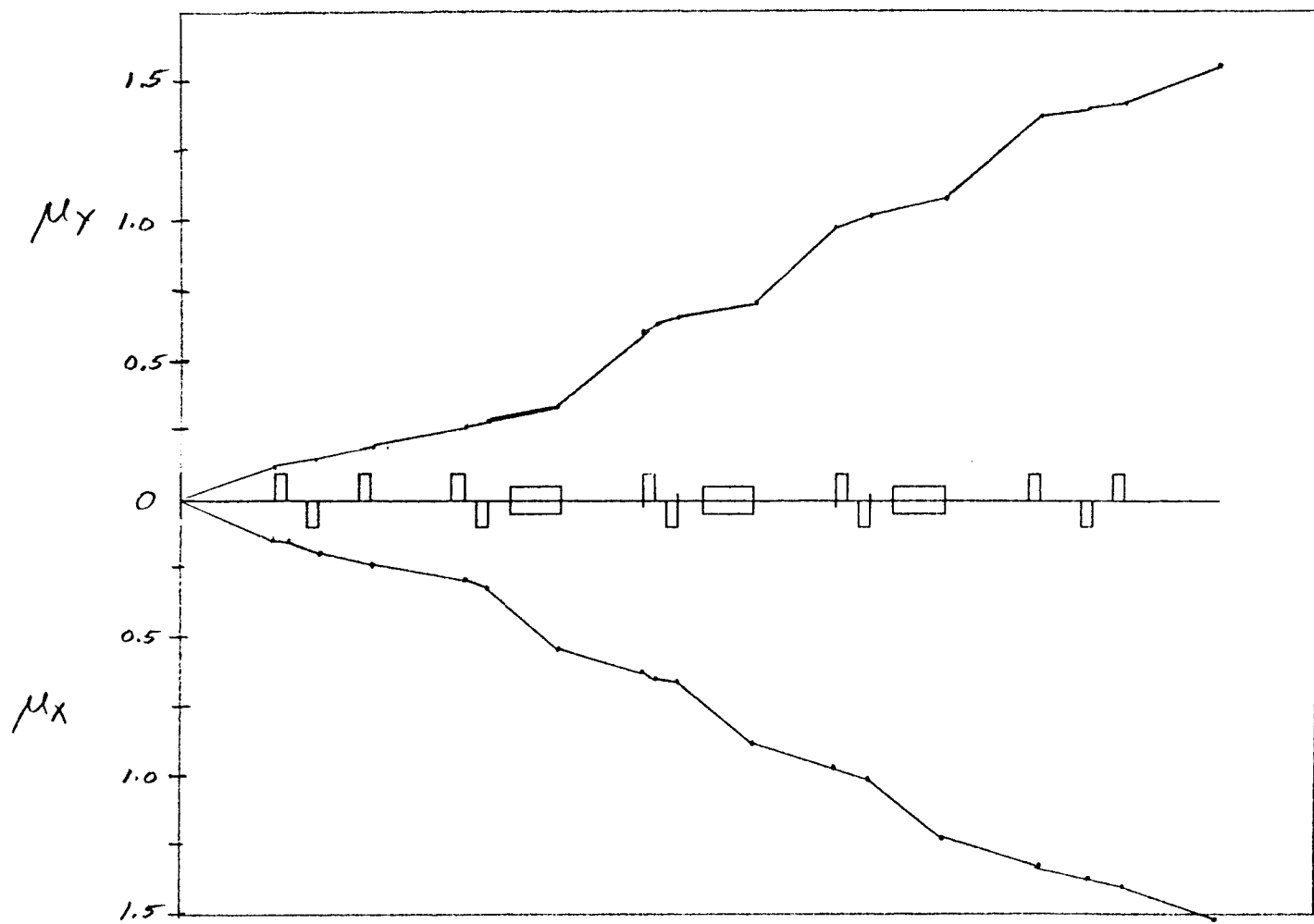


Figure 1(b). Phase Advance for L2V2 Lattice

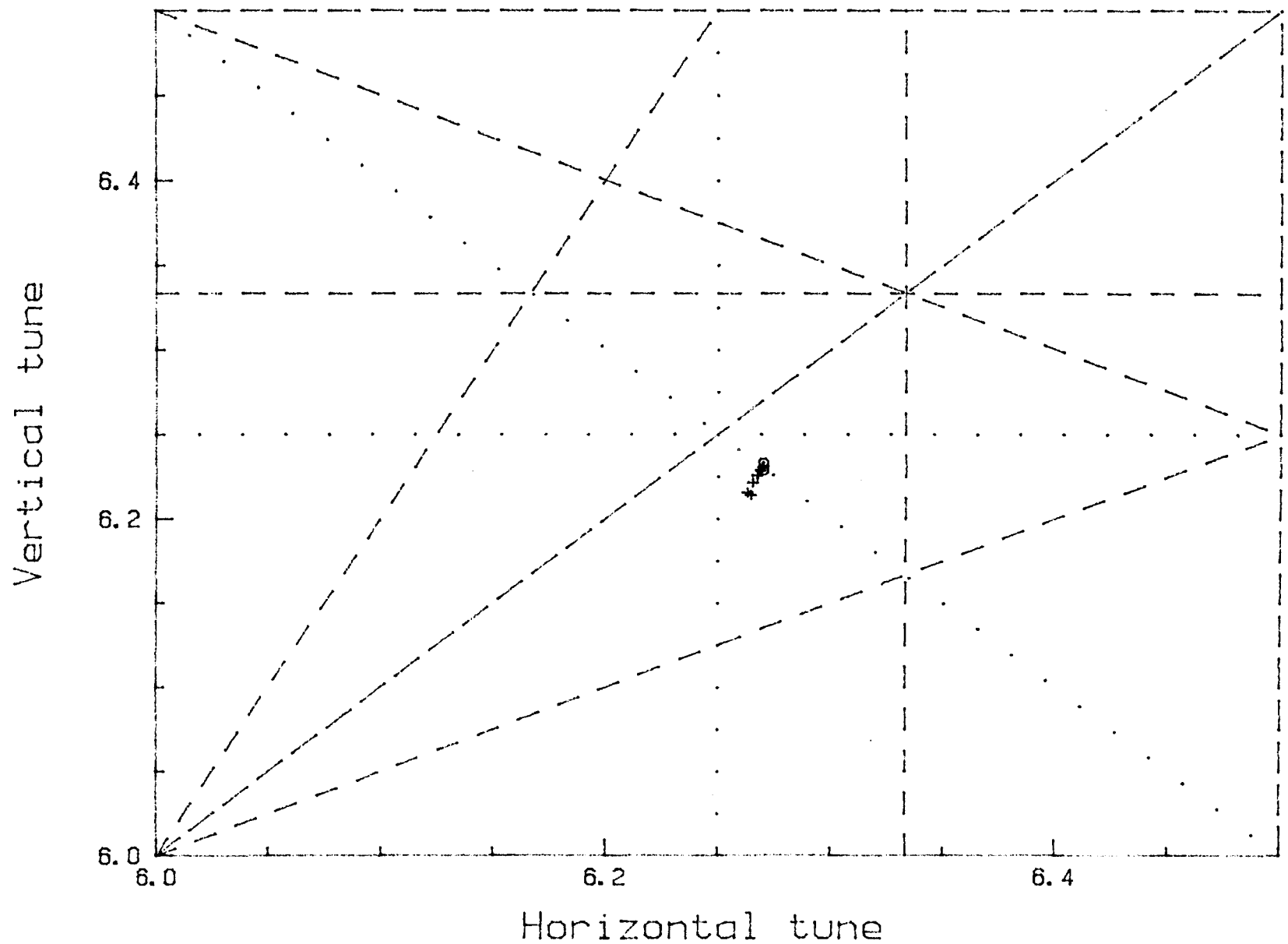


Figure 2. L2V2 Tune Plot

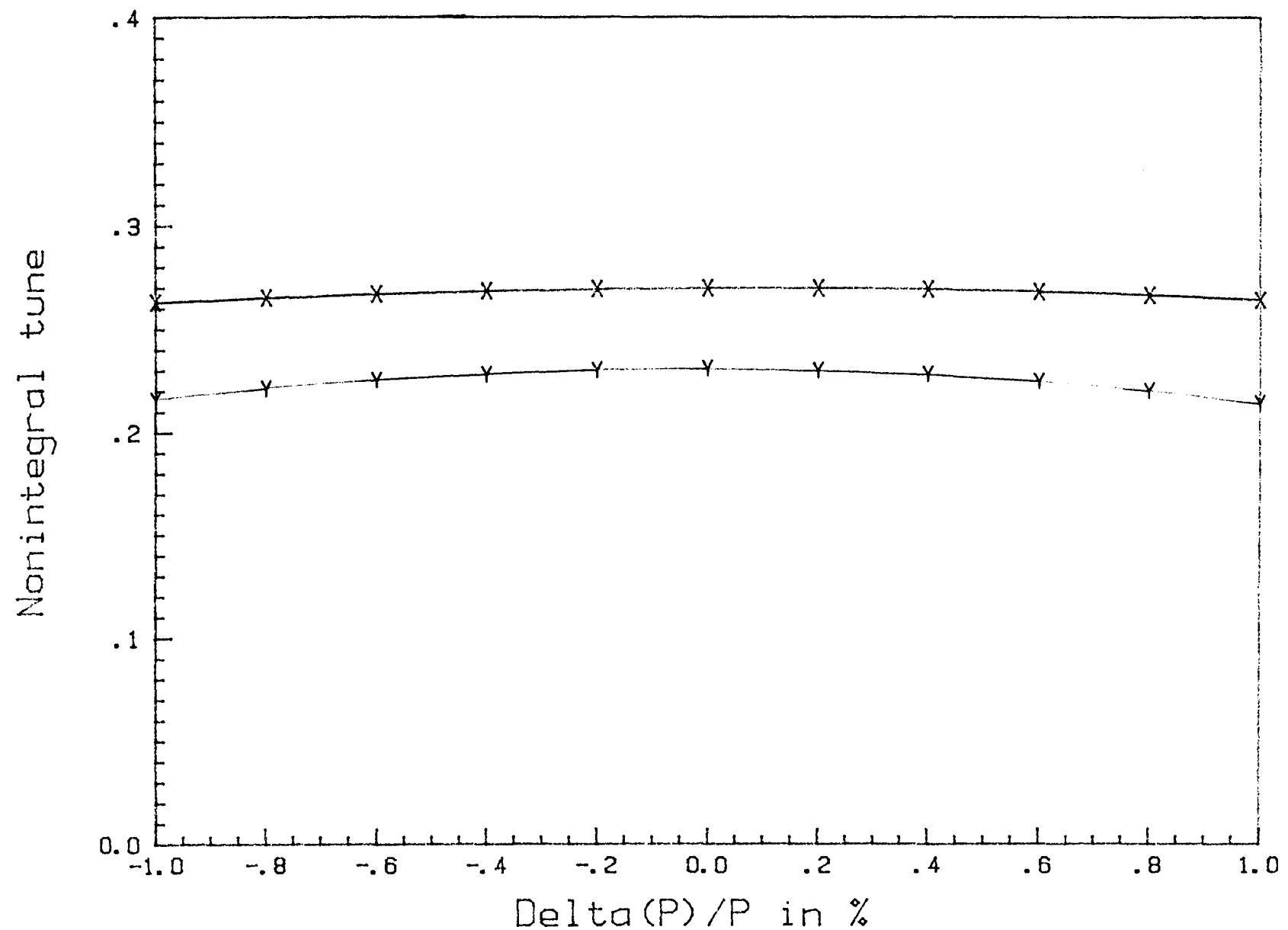


Figure 3. Tune vs Momentum

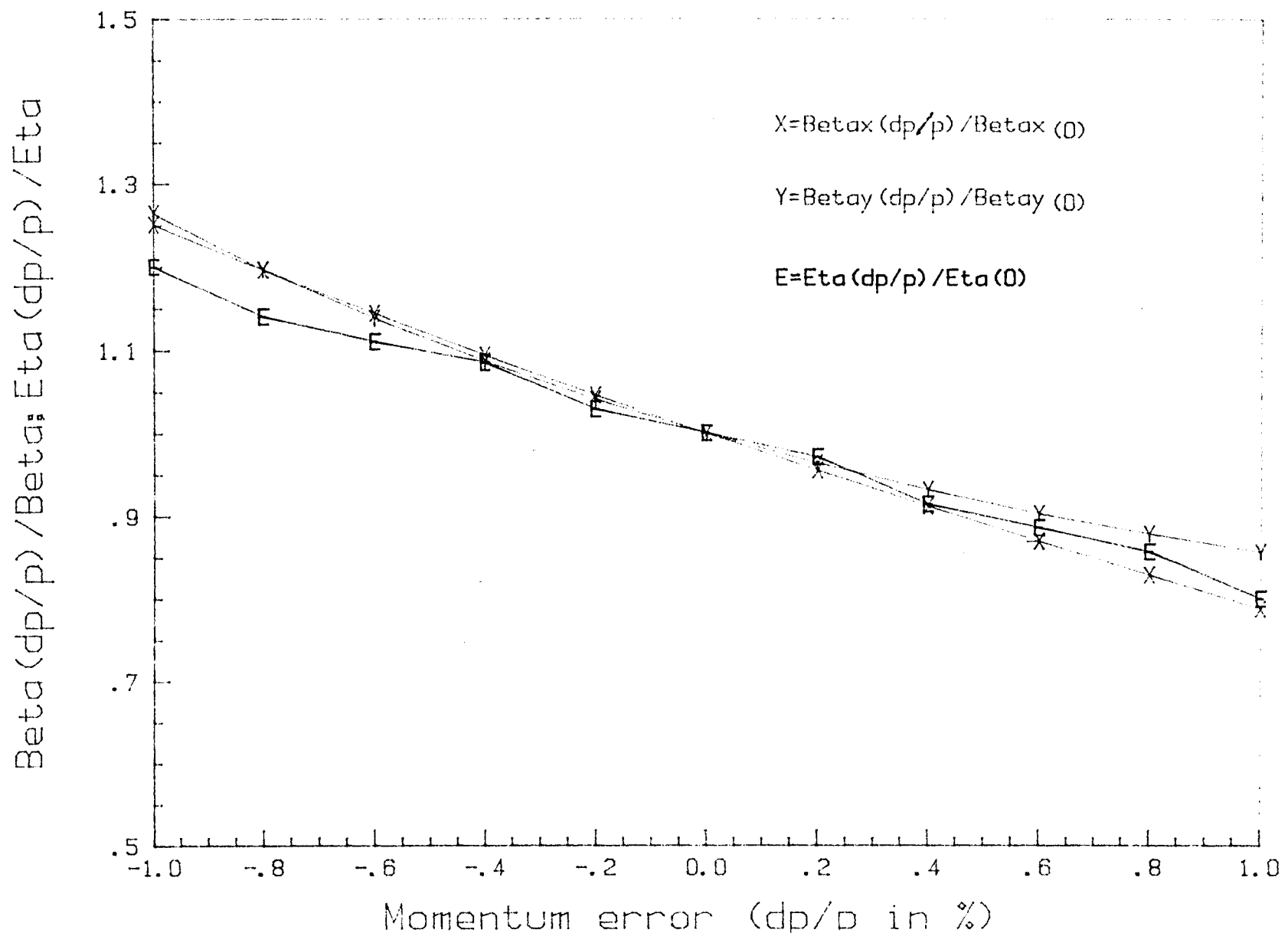


Figure 4. Beta and Eta vs Momentum

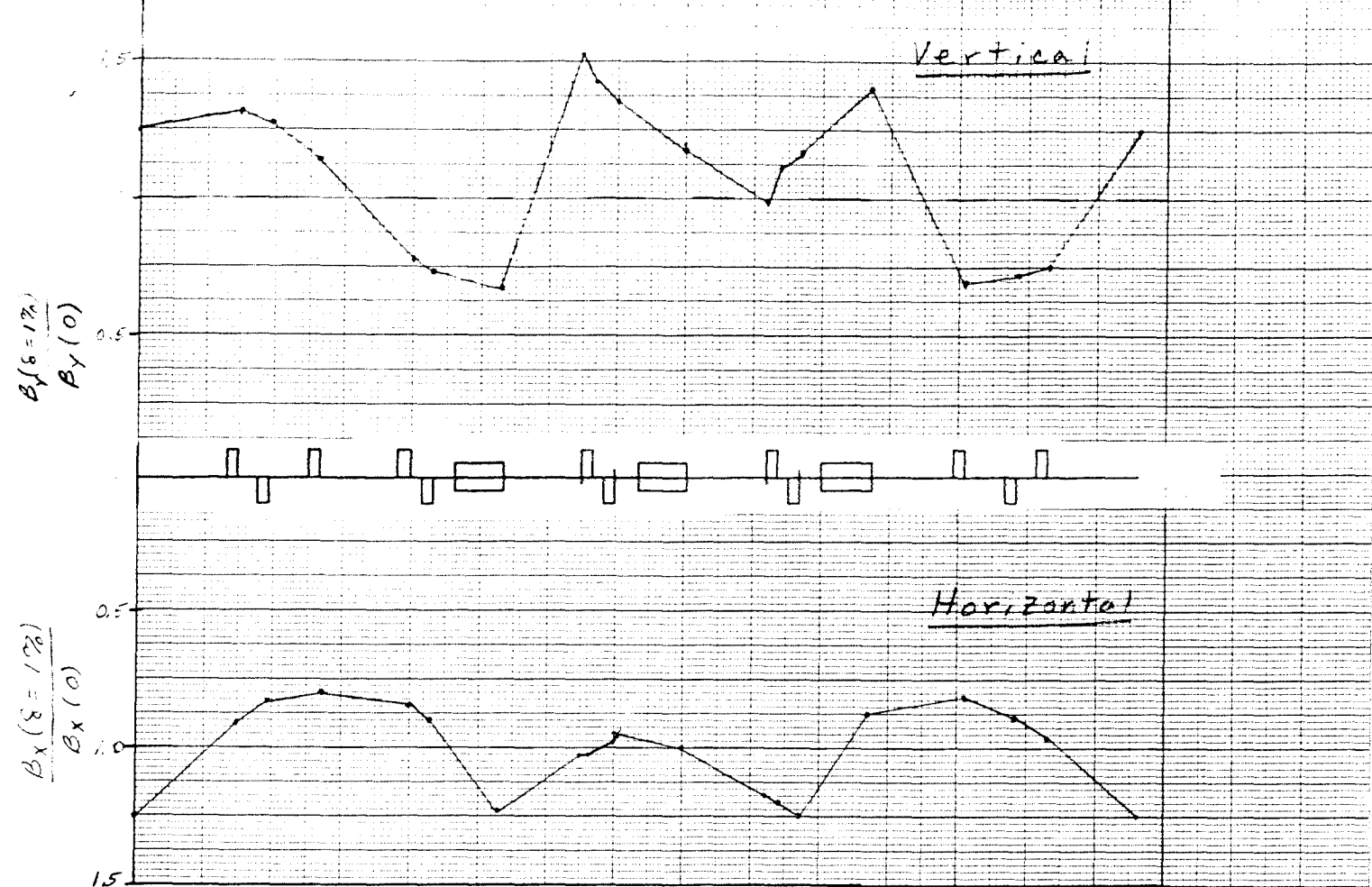


Figure 5. Beta Function Variation for $\delta = \frac{dp}{p} = 1\%$.

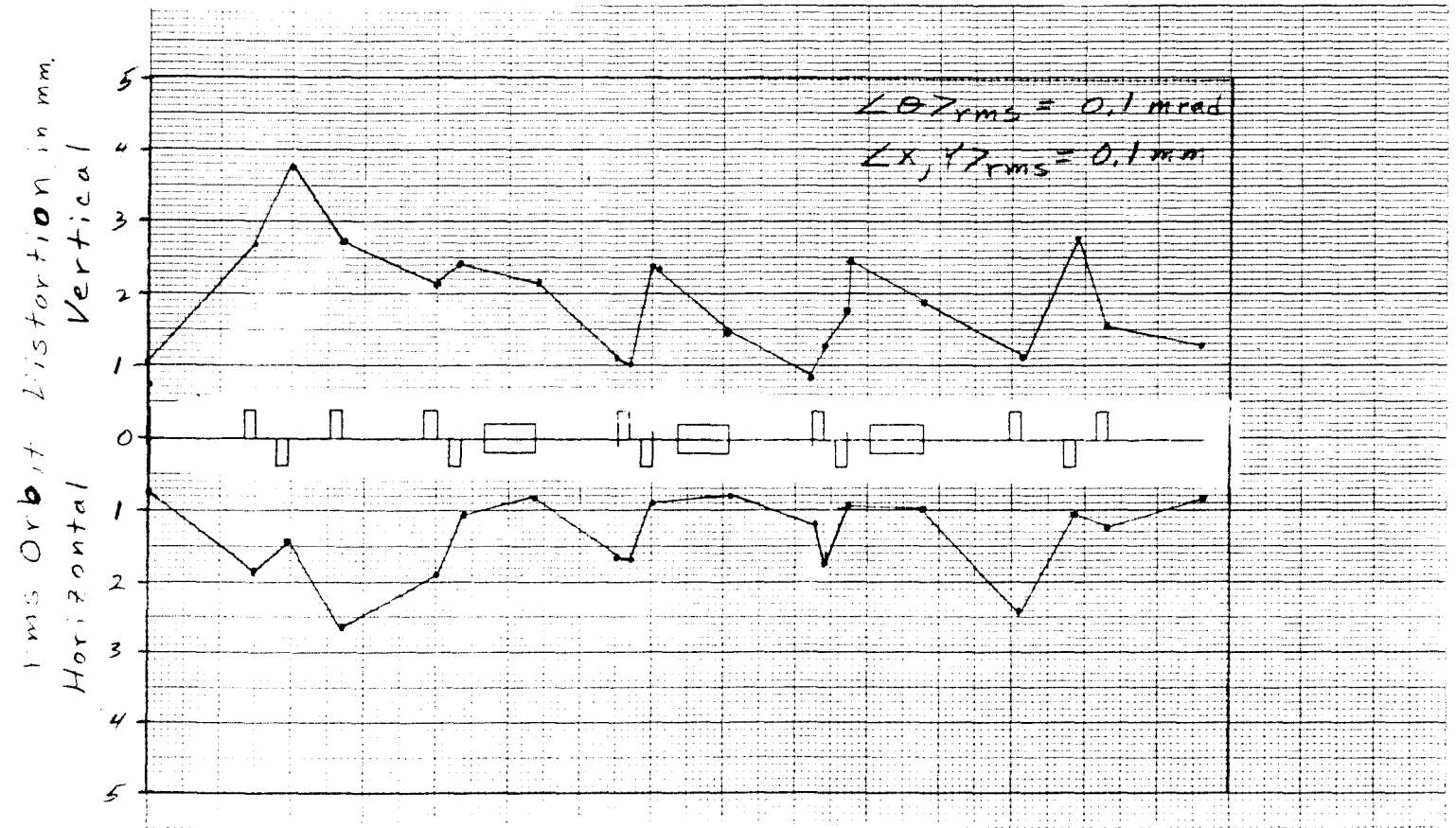


Figure 6. RMS Orbit Distortions for L2V2 Lattice.

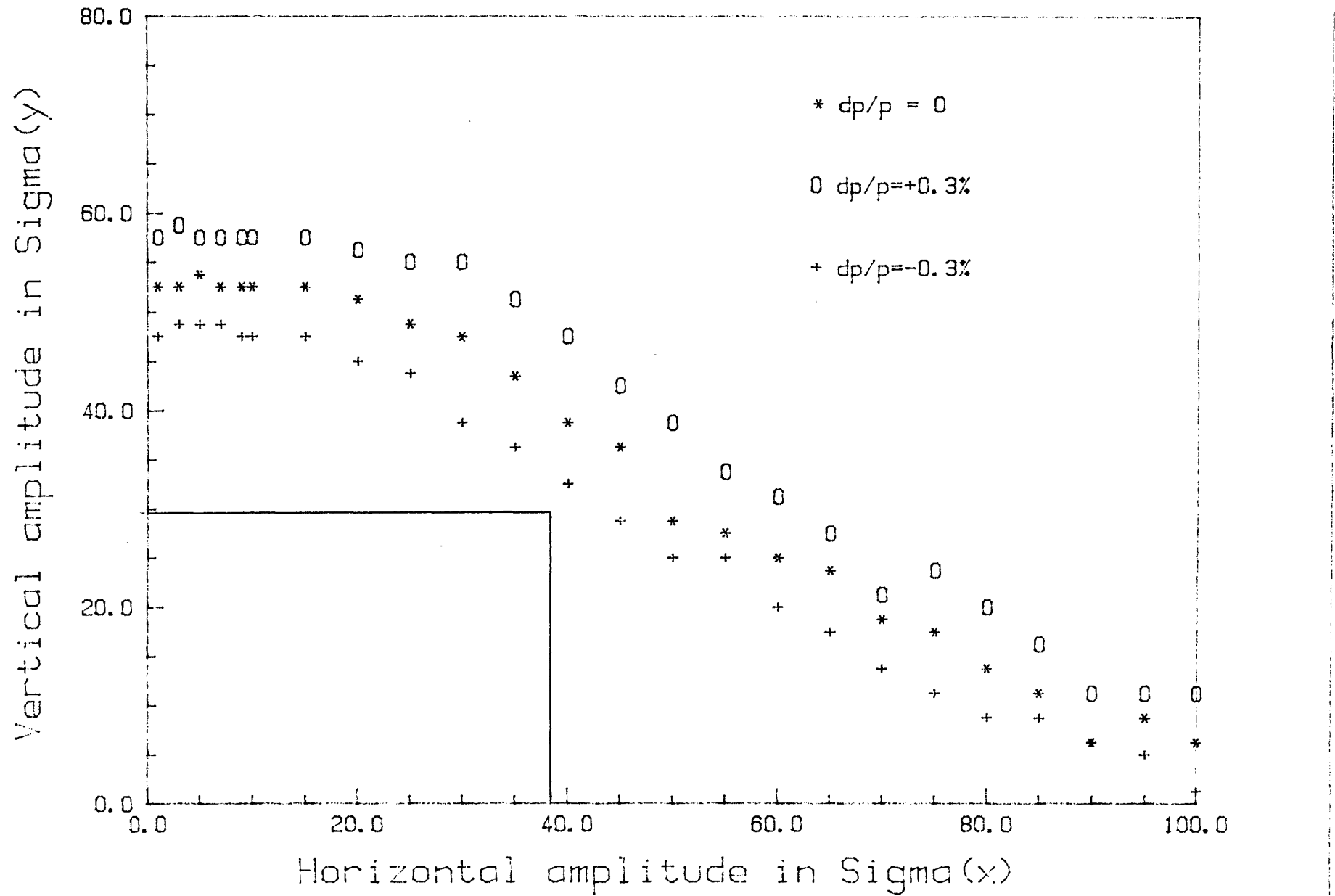


Figure 7. L2V2 Dynamic Aperture

γ' in radians

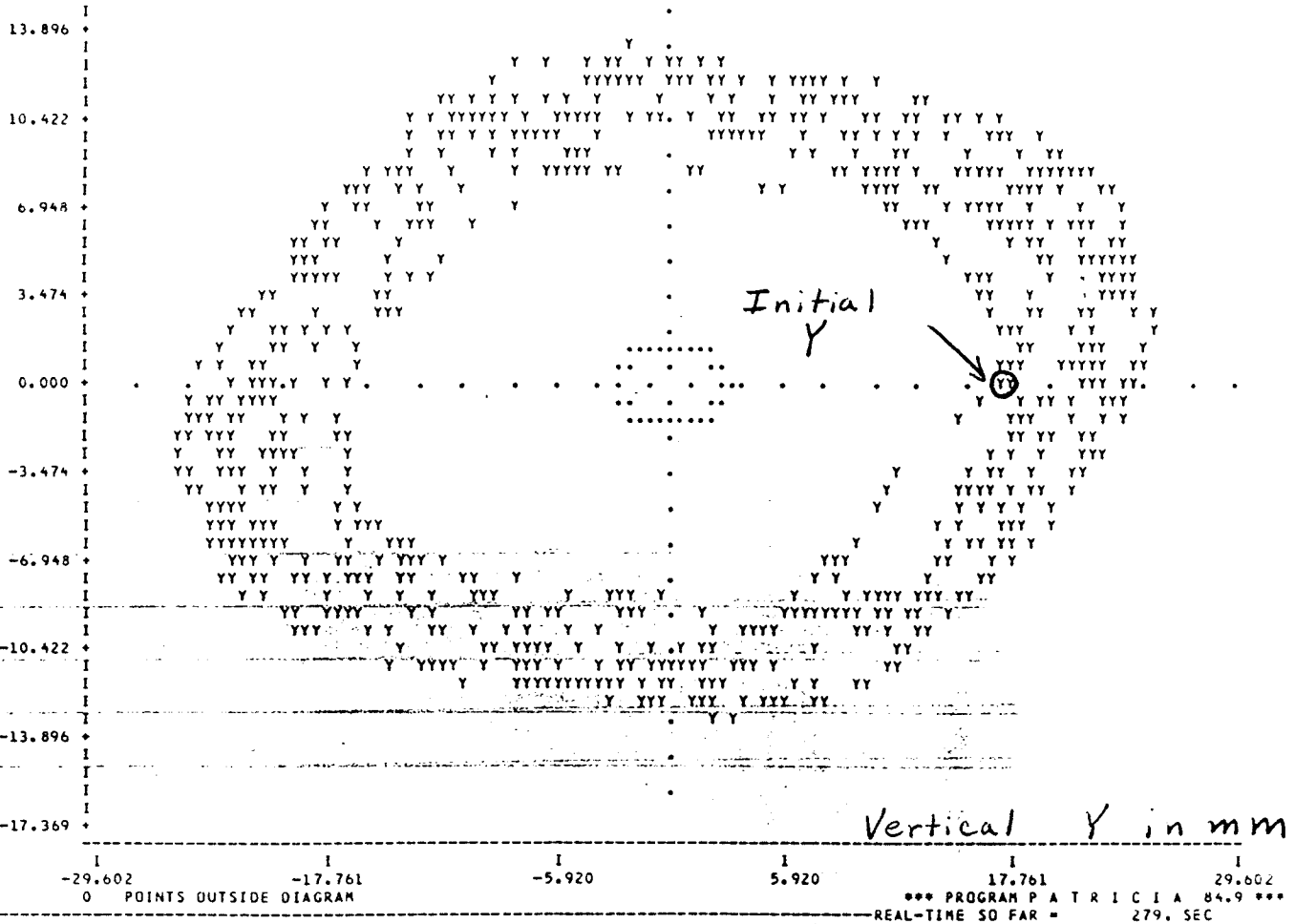
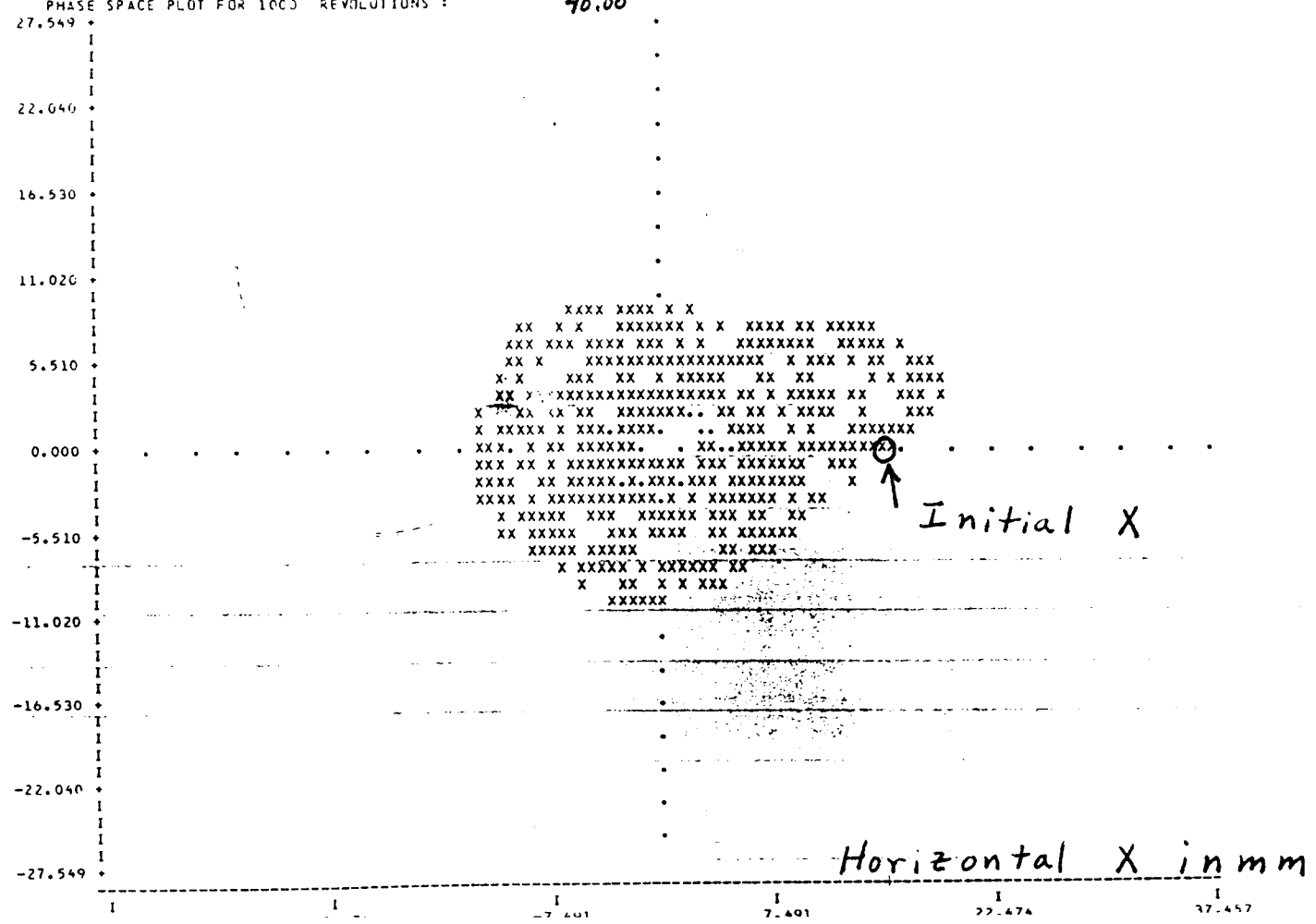


Figure 8. Particle Trajectory for $N_x = N_y = 40$

INITIAL PARAMETERS OF PARTICLE #3 : $x_0 = 14.95\text{MM}$ $x_{PA} = 0.00\text{RAD}$ $y_0 = 16.74\text{MM}$ $y_{PA} = 0.00\text{RAD}$
OR : BETATRON AMPLITUDES = 40.00 SIGMA IN X ; AND ~~40.00~~ SIGMA IN Y ; ENERGY DEVIATION = 0.00 SIGMA AT 1.00 GEV
PHASE SPACE PLOT FOR 1000 REVOLUTIONS : 40.00

X' in radians



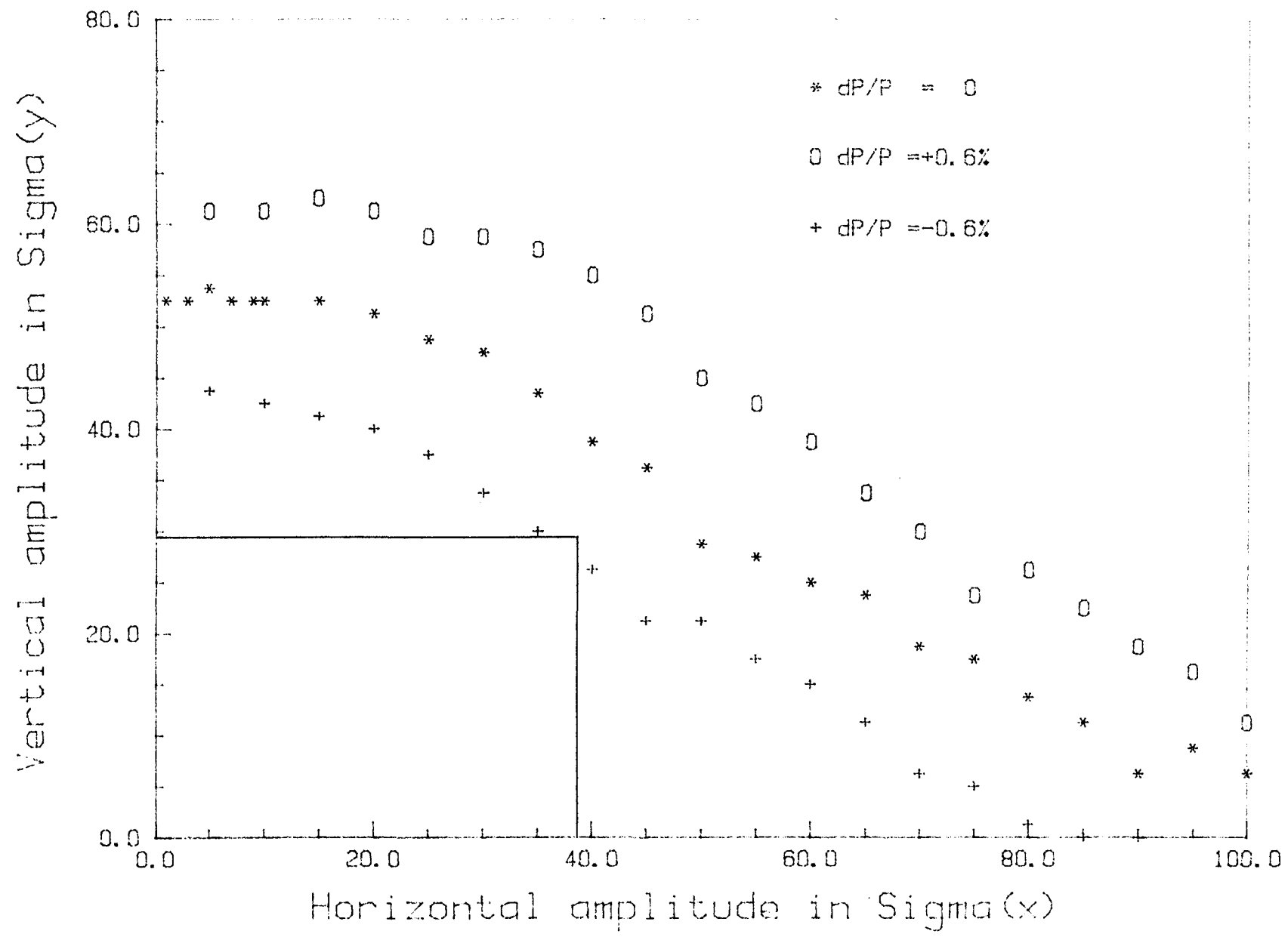


Figure 9. L2V2 Dynamic Aperture

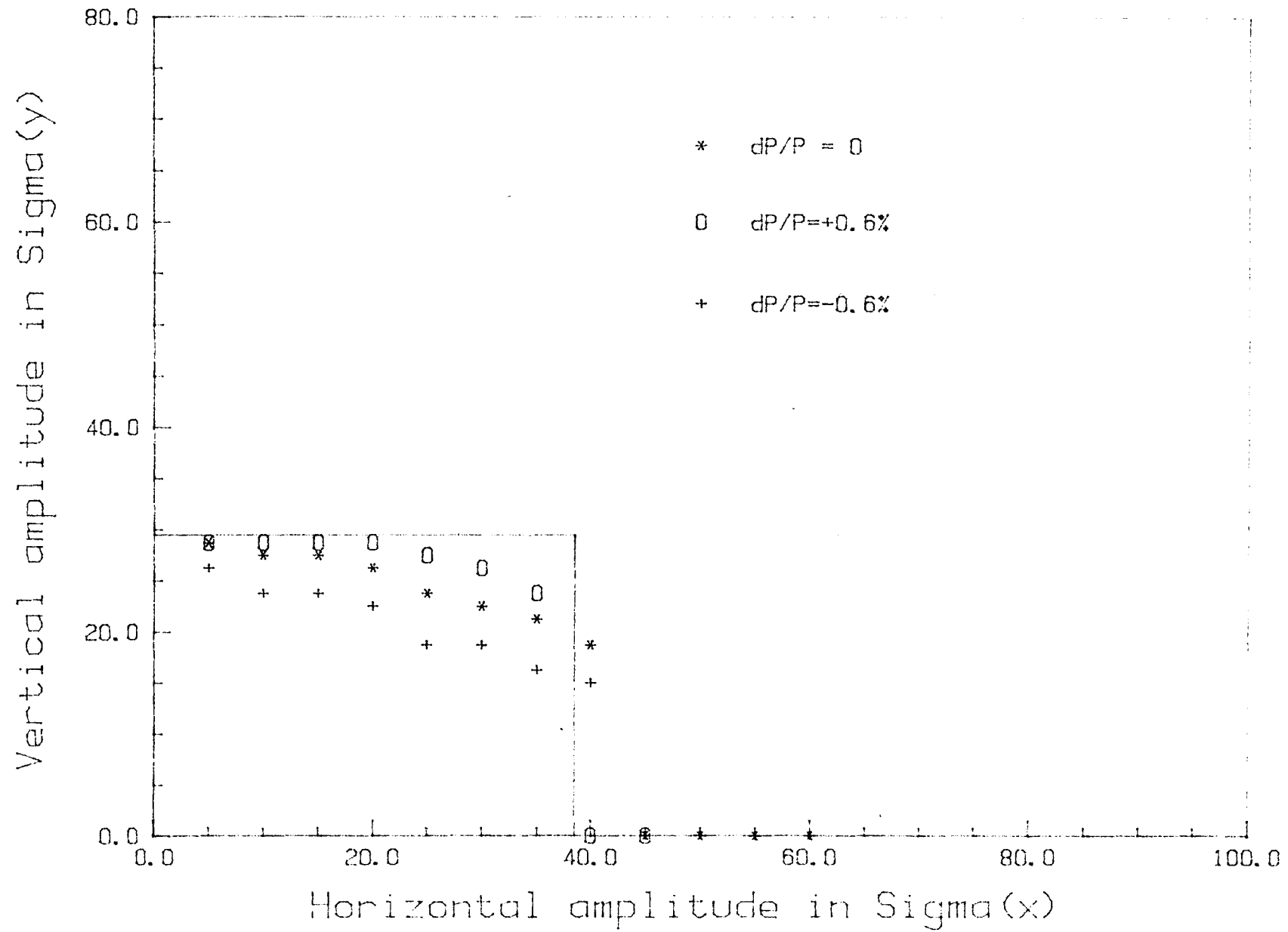


Figure 10. L2V2 Physical Aperture

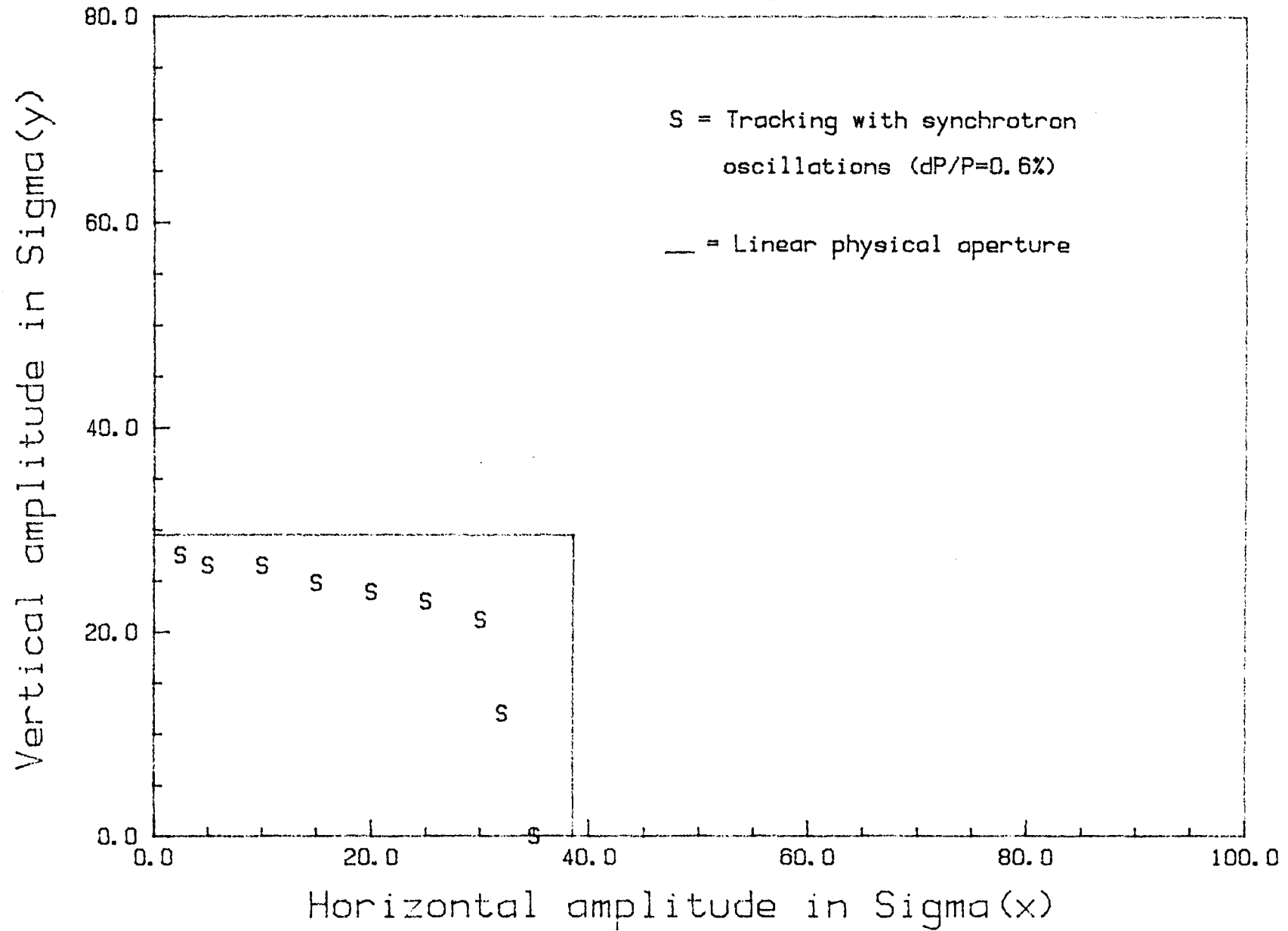


Figure 11. L2V2 Physical Aperture.